Enhanced power absorption of a point absorber wave energy converter using a tuned inertial mass

Ruriko Haraguchi[a], Takehiko Asai[b]

[a]*Graduate School of Systems and Information Engineering, University of Tsukuba, Japan*
[b]*Faculty of Engineering, Information and Systems, University of Tsukuba, Japan*

Abstract

A novel point absorber wave energy converter with a tuned inertial mass (TIM), which is capable of significantly increasing the energy absorption and broadening the effective bandwidth, is proposed in this paper. The mechanism of the TIM has originally been introduced in the field of civil engineering as a passive energy absorber for structures subjected to external loadings such as earthquakes. It relies on attaching an additional tuning spring and a rotational inertial mass to the primary system, to improve the energy absorption performance by amplifying the displacement of the damper. Thus, considering typical point absorbers modeled as a mass-spring-dashpot system similar way to civil structures, the application of the TIM to wave energy converters can be expected to have a significant effect. In this paper, numerical investigation on the power generation performance of a point absorber with the TIM is conducted under random sea waves. The amplitude response and power generation performance are compared with the conventional point absorber, considering both non-resonant and resonant buoy cases. It is shown that by properly designing the tuning spring stiffness and generator damping, the rotation of the generator can be amplified compared to the buoy, increasing the power absorption drastically.

Keywords: Wave energy converter, Point absorber, Tuned inertial mass, Random sea waves

1. Introduction

First stimulated by the oil crisis 40 years ago, harvesting energy from ocean waves is now considered as an alternative approach to meet renewable energy targets [1, 2]. The enormous wave power potential has attracted engineers worldwide with more than 1,000 patents in Japan, North America, and Europe [3],

and among them are oscillating water column, oscillating body, and overtopping devices [4, 5, 6, 7, 8, 9, 10]. Out of these, the point absorber classified as the oscillating body, is considered one of the most promising concepts which make up a great proportion of existing full-scale prototypes. It consists of a floater with dimensions much smaller than the incident wave length, which converts the motion of ocean waves to produce power. Compared to other concepts, point absorbers can exploit more powerful wave regimes available in deep offshore regions, and absorbs energy from all directions. Moreover, the buoys can be combined in arrays to produce sufficient energy for commercial exploitation.

Until now, a great amount of effort has been devoted to improving the efficiency of point absorbers based on mathematical models [11]. It is well known that a point absorber in resonance with the incoming wave has significantly high power absorption due to its enhanced amplitude [12]. However, in practice, this frequency matching meets with serious difficulty because real waves are not single frequency, and the natural frequency of the buoy tends to be much higher than typical ocean wave frequencies for a reasonable size buoy [4, 13]. Therefore, methods to force the system into resonance via active control have been considered. Latching the point absorber at fixed positions to achieve phase control was first proposed by Budal and Falnes [14] and the phase control strategies including latching control and reactive control continue to be an active area of research [15, 16, 17, 18, 19, 20]. This approach requires the prediction of the incoming wave some time in the future, along with solving the complicated control problem to determine the latched time intervals. On the other hand, methods to simply engineer the frequency response of the point absorber have also been considered. Shadmen et al. [21] presented a geometrical optimization method based on tuning the system to oscillate in the range of predominant sea states. Engstrom et al. [22] presented phase control by using a supplementary submerged body to shift the natural frequency of the buoy to coincide with typical sea states. Both of these studies discussed that enhanced amplitude response of the buoy leads to a narrow resonance bandwidth which is in conflict with the desire to correspond to the wide spectrum of ocean waves. Thus, the compromise between maximum power absorption and broad resonance bandwidth has always been an issue associated with the optimization of point absorbers.

In this study, a point absorber with a tuned inertial mass (TIM) is proposed to increase the power absorption and broaden the effective wave frequency range. The TIM has a different configuration from the traditional tuned mass damper (TMD) [23] and the mechanism has originally been introduced in the field of civil engineering as a passive vibration control device for structures subjected to exter-

nal loadings such as earthquakes [24, 25, 26]. It relies on attaching an additional tuning spring and a rotational inertial mass to the primary system, to amplify the displacement of the viscous damper by taking advantage of the resonance effect. In the theory of point absorbers, it is typical to model the power take-off (PTO) system as a linear damper [27], resulting in a mass-spring-dashpot system. Hence, the application of the TIM to point absorbers can be expected to have a significant effect in terms of energy absorption. In contrast to previous studies which couple the PTO with the buoy's oscillation, this study inserts the tuning spring which de-couples the PTO from the buoy's oscillation and couples with the oscillation of the rotational inertial mass. Therefore, by appropriately designing the tuning spring, rotational inertial mass, and damping coefficient, the rotation number of the rotational inertial mass can be amplified compared to the buoy, which increases the displacement of the PTO to achieve substantial power absorption.

The objective of this paper is to verify the effectiveness of applying the TIM to a point absorber. First, in Section 2, the theoretical models of the conventional system and proposed system with the TIM are developed, following the modeling of stochastic sea states using the JONSWAP spectrum. Then, in Section 3, the state-space representation is given to evaluate the amplitude response along with the power generation. Finally, in Section 4, numerical studies are carried out focussing on the optimization of design parameters, amplitude response, and power generation of the proposed system compared with the conventional system.

2. Modeling

2.1. Point absorber with tuned inertial mass

We begin by reviewing the conventional point absorber illustrated in Fig. 1(a). A semi-submerged cylinder with diameter D and draft L is considered as the wave interacting part of a point absorber. The generator is anchored rigidly to the ocean floor, and the supporting spring with stiffness k_s is used to prevent the wire from sagging. For simplicity, we consider the heave motion only as this becomes dominant for the power extraction of wave energy [28].

Let z be the vertical displacement of the buoy from its equilibrium state. Since the displacement of the buoy is coupled with the rotation of the generator, the conventional point absorber can be modeled as a single-degree-of freedom (SDOF) system with the following equation of motion:

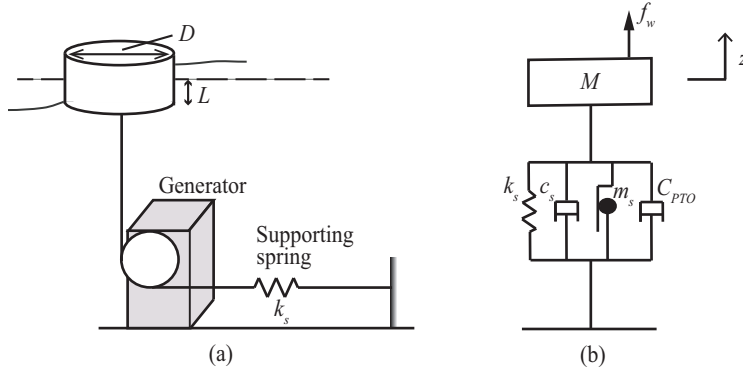$$(M + m_s)\ddot{z} + c_s\dot{z} + k_s z = f_w - u \tag{1}$$

3

Figure 1: Conventional point absorber (SDOF system): (a) Schematic illustration, (b) Model.
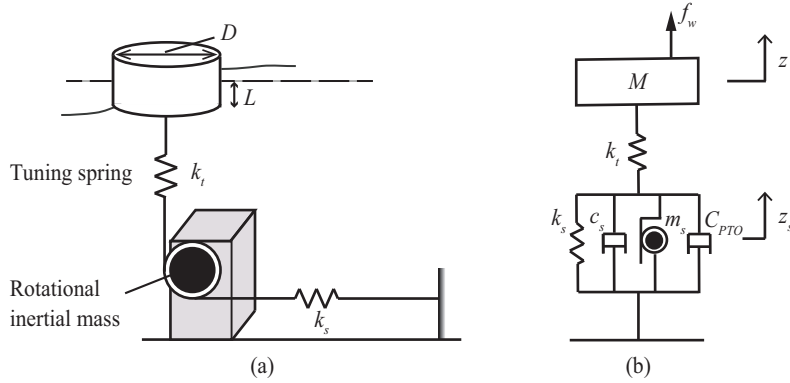

Figure 2: Point absorber with tuned inertial mass (TIM system): (a) Schematic illustration, (b) Model.

where M is the buoy mass, m_s is the inertial mass of the generator and pulley, c_s is the mechanical damping including friction, u is the electromagnetic damping force which acts as a control force given by

$$u = C_{PTO}\dot{z} \qquad (2)$$

and f_w is the hydrodynamic force acting on the cylinder. The corresponding model is shown in Fig. 1(b).

Based on linear potential wave theory, the hydrodynamic force f_w is described by

$$f_w = f_a + f_b + f_c \qquad (3)$$

4

where f_a is the excitation force, f_b is the hydrostatic force due to buoyancy, and f_c is the radiation force. The relation between the excitation force f_a and the amplitude of the incident wave a is given in the frequency domain using a transfer function $F_a(\omega)$ as

$$\hat{f}_a(\omega) = F_a(\omega)\hat{a}(\omega) \tag{4}$$

Note that $\hat{f}(\omega)$ denotes the Fourier transform of a function $f(t)$. The hydrostatic force becomes a linear function of z given as

$$f_b = -K_w z \tag{5}$$

where K_w is given with the gravity acceleration g and sea water density ρ by

$$K_w = \rho g \pi \left(\frac{D}{2}\right)^2 \tag{6}$$

and the radiation force f_c is given as

$$\hat{f}_c(\omega) = -(j\omega m_a(\omega) + c_r(\omega))\hat{z} \tag{7}$$

where $m_a(\omega)$ is the added mass and $c_r(\omega)$ is the radiation damping.

Next, to increase the power absorption and widen the effective bandwidth, a point absorber with TIM is proposed. As illustrated in Fig. 2(a), a tuning spring is installed between the buoy and generator, and a relatively small physical mass which rotates with the generator is attached. When the vertical motion is transformed into rotary motion, the small physical mass can produce an amplified equivalent mass effect on the order of a thousandfold due to the rotary inertia [24]. As shown in Fig. 2(b), the proposed system is modeled as a two-degree-of-freedom (2DOF) system, noting that the rotational displacement of the inertial mass is coupled with the generator.

Defining z, z_s, and z_t as the displacement of the buoy, rotational inertial mass, and the elongation of the tuning spring, respectively, the relationship among these variables are given by

$$z = z_s + z_t \tag{8}$$

The equations of motion for the proposed TIM system are derived as

$$M\ddot{z} = f_w - f_t \tag{9}$$
$$m_s\ddot{z}_s + c_s\dot{z}_s + k_s z_s = f_t - u \tag{10}$$

5

where f_t is the force from the tuning spring and the the electromagnetic damping force is defined by

$$u = C_{PTO}\dot{z}_s \tag{11}$$

in this case. Also, denoting the stiffness of the tuning spring as k_t, this force becomes proportional to the relative displacement given as

$$f_t = k_t z_t = k_t(z - z_s) \tag{12}$$

2.2. Power take-off system

In this study, the generator is assumed to be a three-phase permanent magnet synchronous machine, interfaced with a centralized DC power bus. For this assumption, it is reasonable to assume that the quadrature field is explicitly controlled to regulate power conversion while the direct stator field is maintained at zero. Thus, the three phase voltage and current vectors are transformed to "quadrature components", i.e., effective scalar quantities are used for the back-EMF v and corresponding current i. More details can be found in [29, 30]. Assuming an ideal generator with linear behavior and minimal core loss, results in linearity between the back-EMF and the velocity coupled with the generator. Therefore, the equation is defined separately for the conventional system and TIM system, given as

$$v = K_e \dot{z}, \quad v = K_e \dot{z}_s \tag{13}$$

respectively, where K_e is a constant associated with the back-EMF of the generator. By reciprocity, the electromagnetic force and generator current has the following linear relationship

$$u = -K_e i \tag{14}$$

In the study of wave energy converters (WECs), it is common to assume viscous dampers in place of the PTO system. This constitutes the imposition of a feedback law

$$i = -Yv \tag{15}$$

where Y is the admittance of the generator. Applying this to Eq. (14) with Eq. (13) yields

$$u = YK_e^2 \dot{z}, \quad u = YK_e^2 \dot{z}_s \tag{16}$$

for the individual systems. Thus the generator damping C_{PTO} for both cases can be given as

$$C_{PTO} = YK_e^2 \tag{17}$$

expressing how the generator damping, i.e., the electromagnetic damping force u is controlled by the admittance Y.

2.3. Stochastic sea state model

In simple theoretical models of WECs, it is typical to assume the incident waves to be regular. For a more realistic model, irregular waves are used with time-domain analysis which requires much more computing time [4]. An alternative method with less computation for modeling true sea states is the stochastic modeling. We assume the wave amplitude $a(t)$ to be a stationary stochastic process with spectral density $S_a(\omega)$ and variance given by

$$\sigma_a{}^2 = \frac{1}{2\pi} \int_{-\infty}^{\infty} S_a(\omega) d\omega \tag{18}$$

Characterizing $S_a(\omega)$ by the JONSWAP spectrum [31] with peak wave period T_p, significant wave height H_s, and peak enhancement factor γ derives the following

$$S_a(\omega) = 310\pi \frac{H_s^2}{T_p^4 \omega^5} \exp\left[\frac{-944}{T_p^4 \omega^4}\right] \gamma^Y \tag{19}$$

where

$$Y = \exp\left[-\left(\frac{0.191\omega T_p - 1}{\sqrt{2}\phi}\right)^2\right] \tag{20}$$

and

$$\phi = \begin{cases} 0.07: & \omega T_p \leq 5.24 \\ 0.09: & \omega T_p > 5.24 \end{cases} \tag{21}$$

The peak enhancement factor γ is constrained by $1 \leq \gamma \leq 3.3$, with $\gamma = 1$ describing a fully developed sea.

To model the wave amplitude, we find a finite-dimensional noise filter

$$F_w \sim \left[\begin{array}{c|c} \mathbf{A}_w & \mathbf{B}_w \\ \hline \mathbf{C}_w & \mathbf{0} \end{array}\right] \tag{22}$$

such that its power spectrum is close to the JONSWAP spectrum, i.e., $S_a(\omega) \approx |F_w(\omega)|^2$, for a unit intensity white noise input. It should be noted that we make use of the short-hand $\mathbf{G} \sim \left[\begin{array}{c|c} \mathbf{A} & \mathbf{B} \\ \hline \mathbf{C} & \mathbf{D} \end{array}\right]$ to imply $\mathbf{G}(s) = \mathbf{C}[s\mathbf{I} - \mathbf{A}]^{-1}\mathbf{B} + \mathbf{D}$ in this article.

According to the simplified procedure advocated by Spanos [32], F_w can be approximated by a fourth-order controllable canonical form of

$$\mathbf{A}_w = \begin{bmatrix} 0 & 1 & 0 & 0 \\ 0 & 0 & 1 & 0 \\ 0 & 0 & 0 & 1 \\ a_1 & a_2 & a_3 & a_4 \end{bmatrix}, \quad \mathbf{B}_w = \begin{bmatrix} 0 \\ 0 \\ 0 \\ 1 \end{bmatrix}, \quad \mathbf{C}_w = \begin{bmatrix} 0 & 0 & c_3 & 0 \end{bmatrix} \tag{23}$$
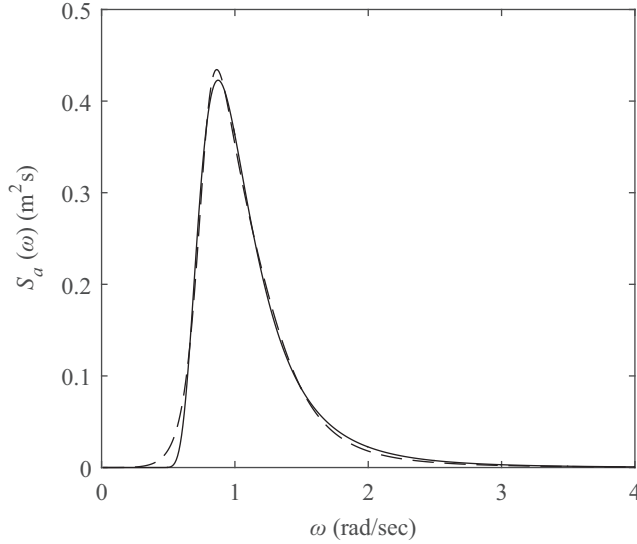
7

Figure 3: Example of Jonswap spectrum with $T_p = 6$ s, $H_s = 1$ m, $\gamma = 1$ (solid) and the spectrum of the fourth order finite dimensional approximate system (dashed).

where the filter parameters a_1, a_2, a_3, a_4, and c_3 are chosen to minimize the mean-square error $\int_{-\infty}^{\infty}(S_a(\omega) - |F_w(\omega)|^2)^2 d\omega$, while constraining a_1 through a_4 so that the system poles are in the open left half plane. Fig. 3 shows an example of a JONSWAP spectrum for $T_p = 6$ s, $H_s = 1$ m, $\gamma = 1$ and its fourth-order finite-dimensional approximate system. We can confirm in the figure that the fourth-order F_w estimates the JONSWAP spectrum very well.

3. State-space representation

In this section, to evaluate the amplitude response and assess the power generation for stochastic sea states, a state-space form of the proposed device with TIM is developed. The derivation of the state-space form for the conventional point absorber can be found in [33], which is not delved into in this paper.

3.1. Amplitude response of buoy and rotational inertial mass

In the following, the equations of motion for the buoy and rotational inertial mass are expressed in state-space form separately, and then augmented to assess the amplitude response relating the wave elevation.

8

Taking into account the hydrodynamics acting on the buoy, we take the Fourier transform of Eq. (9) with Eqs. (3), (4), (5), and (7) inserted, which gives the transfer function relating a and f_t to z as

$$\hat{z} = G_a(\omega)\hat{a} + G_f(\omega)\hat{f}_t \tag{24}$$

where

$$G_a(\omega) = \frac{F_a(\omega)}{-\omega^2(M + m_a(\omega)) + i\omega c_r(\omega) + K_w} \tag{25}$$

$$G_f(\omega) = -\frac{1}{-\omega^2(M + m_a(\omega)) + i\omega c_r(\omega) + K_w} \tag{26}$$

The infinite-dimensional systems G_a and G_f are approximated into finite-dimensional systems, i.e.,

$$G_a \sim \left[\begin{array}{c|c} \mathbf{A}_a & \mathbf{B}_a \\ \hline \mathbf{C}_a & \mathbf{0} \end{array}\right], \quad G_f \sim \left[\begin{array}{c|c} \mathbf{A}_f & \mathbf{B}_f \\ \hline \mathbf{C}_f & \mathbf{0} \end{array}\right] \tag{27}$$

We must note, the function $F_a(\omega)$ in Eq. (25) is noncausal which will be problematic when approximating $G_a(\omega)$ by a finite-dimensional state-space. Therefore the technique of spatial delay proposed by Falnes [34] is used, defining a as the wave amplitude at a distance of d in front of the buoy. Once Eq. (27) is obtained, the identified systems are augmented as

$$\begin{bmatrix} G_a & G_f \end{bmatrix} \sim \left[\begin{array}{c|cc} \mathbf{A}_m & \mathbf{B}_m & \mathbf{E}_m \\ \hline \mathbf{C}_m & \mathbf{0} & \mathbf{0} \end{array}\right] \tag{28}$$

where the augmented matrices $\mathbf{A}_m$, $\mathbf{B}_m$, $\mathbf{E}_m$, and $\mathbf{C}_m$ are

$$\mathbf{A}_m = \begin{bmatrix} \mathbf{A}_a & \mathbf{0} \\ \mathbf{0} & \mathbf{A}_f \end{bmatrix}, \quad \mathbf{B}_m = \begin{bmatrix} \mathbf{B}_a \\ \mathbf{0} \end{bmatrix}, \quad \mathbf{E}_m = \begin{bmatrix} \mathbf{0} \\ \mathbf{B}_f \end{bmatrix}, \quad \mathbf{C}_m = \begin{bmatrix} \mathbf{C}_a & \mathbf{C}_f \end{bmatrix} \tag{29}$$

and the equivalent state-space representation is

$$\dot{\mathbf{x}}_m = \mathbf{A}_m\mathbf{x}_m + \mathbf{B}_m a + \mathbf{E}_m f_t \tag{30}$$

$$z = \mathbf{C}_m\mathbf{x}_m \tag{31}$$

On the other hand, the equation of motion for the rotational inertial mass in Eq. (10) can be transformed into state-space form directly. Defining the state vector as $\mathbf{x}_n = \begin{bmatrix} z_s & \dot{z}_s \end{bmatrix}^T$ gives

$$\dot{\mathbf{x}}_n = \mathbf{A}_n\mathbf{x}_n + \mathbf{B}_n i + \mathbf{E}_n f_t \tag{32}$$

9

where

$$\mathbf{A}_n = \begin{bmatrix} 0 & 1 \\ -\frac{k_s}{m_s} & -\frac{c_s}{m_s} \end{bmatrix}, \quad \mathbf{B}_n = \begin{bmatrix} 0 \\ \frac{K_e}{m_s} \end{bmatrix}, \quad \mathbf{E}_n = \begin{bmatrix} 0 \\ \frac{1}{m_s} \end{bmatrix} \tag{33}$$

Now that the state-space form for the buoy and rotational inertial mass are determined, Eqs. (30) and (32) can be augmented by defining $\mathbf{x}_h = \begin{bmatrix} \mathbf{x}_m^T & \mathbf{x}_n^T \end{bmatrix}^T$ as

$$\dot{\mathbf{x}}_h(t) = \mathbf{A}_h\mathbf{x}_h + \mathbf{B}_h i + \mathbf{E}_h f_t + \mathbf{G}_h a \tag{34}$$

where

$$\mathbf{A}_h = \begin{bmatrix} \mathbf{A}_m & \mathbf{0} \\ \mathbf{0} & \mathbf{A}_n \end{bmatrix}, \quad \mathbf{B}_h = \begin{bmatrix} \mathbf{0} \\ \mathbf{B}_n \end{bmatrix}, \quad \mathbf{E}_h = \begin{bmatrix} \mathbf{E}_m \\ \mathbf{E}_n \end{bmatrix}, \quad \mathbf{G}_h = \begin{bmatrix} \mathbf{B}_m \\ \mathbf{0} \end{bmatrix} \tag{35}$$

The generator current and the force from the supporting spring can be expressed using the state variable $\mathbf{x}_h$ as

$$i = -Yv = -Y\mathbf{C}_h\mathbf{x}_h \tag{36}$$
$$f_t = k_t(z - z_s) = k_t\mathbf{T}_h\mathbf{x}_h \tag{37}$$

where

$$\mathbf{C}_h = \begin{bmatrix} \mathbf{0} & K_e \end{bmatrix}, \quad \mathbf{T}_h = \begin{bmatrix} \mathbf{C}_m & -1 & 0 \end{bmatrix} \tag{38}$$

Thus, when the design parameters Y and k_t are determined, the amplitude response of the buoy and rotational inertial mass to the wave elevation can be assessed by defining a transfer function for each. Substituting Eqs. (36) and (37) into Eq. (34) yields the closed loop system

$$\dot{\mathbf{x}}_h = (\mathbf{A} - Y\mathbf{B}_h\mathbf{C}_h + k_t\mathbf{E}_h\mathbf{T}_h)\mathbf{x}_h + \mathbf{G}_h a \tag{39}$$
$$z = \mathbf{C}_b\mathbf{x}_h \tag{40}$$
$$z_s = \mathbf{C}_r\mathbf{x}_h \tag{41}$$

where

$$\mathbf{C}_b = \begin{bmatrix} \mathbf{C}_m & \mathbf{0} \end{bmatrix}, \quad \mathbf{C}_r = \begin{bmatrix} 0 & 1 & 0 \end{bmatrix} \tag{42}$$

Therefore, the transfer function from the wave elevation to the buoy displacement is given as

$$H_b(s) = \mathbf{C}_b[s\mathbf{I} - \mathbf{A} + Y\mathbf{B}_h\mathbf{C}_h - k_t\mathbf{E}_h\mathbf{T}_h]^{-1}\mathbf{G}_h \tag{43}$$

Similarly, the transfer function from the wave elevation to the rotational displacement of the inertial mass is given as

$$H_r(s) = \mathbf{C}_r[s\mathbf{I} - \mathbf{A} + Y\mathbf{B}_h\mathbf{C}_h - k_t\mathbf{E}_h\mathbf{T}_h]^{-1}\mathbf{G}_h \tag{44}$$

3.2. Power generation

The stochastic sea state model in Eq. (22) combined with the WEC dynamics in Eq. (34) yields the following augmented system, with state vector $\mathbf{x} = \begin{bmatrix} \mathbf{x}_h^T & \mathbf{x}_w^T \end{bmatrix}^T$ as

$$\dot{\mathbf{x}} = \mathbf{A}\mathbf{x} + \mathbf{B}i + \mathbf{F}f_t + \mathbf{G}w \tag{45}$$

where

$$\mathbf{A} = \begin{bmatrix} \mathbf{A}_h & \mathbf{G}_h\mathbf{C}_w \\ \mathbf{0} & \mathbf{A}_w \end{bmatrix}, \quad \mathbf{B} = \begin{bmatrix} \mathbf{B}_h \\ \mathbf{0} \end{bmatrix}, \quad \mathbf{F} = \begin{bmatrix} \mathbf{E}_h \\ \mathbf{0} \end{bmatrix}, \quad \mathbf{G} = \begin{bmatrix} \mathbf{0} \\ \mathbf{B}_w \end{bmatrix} \tag{46}$$

and $w(t)$, the input to the noise filter, is white noise with unit intensity. Eqs. (36) and (37) can be rewritten as

$$i = -Yv = -Y\mathbf{C}\mathbf{x} \tag{47}$$

$$f_t = k_t(z - z_s) = k_t\mathbf{T}\mathbf{x} \tag{48}$$

where

$$\mathbf{C} = \begin{bmatrix} \mathbf{C}_h & \mathbf{0} \end{bmatrix}, \quad \mathbf{T} = \begin{bmatrix} \mathbf{T}_h & \mathbf{0} \end{bmatrix} \tag{49}$$

In this paper, the total power generation is defined as the extracted power minus the electrical loss [29], i.e.,

$$P_g = -iv - P_d \tag{50}$$

where P_d is the electrical loss dominated by conductive dissipation. While the expression for P_d depends on many parameters of the electronic hardware, we make the simplifying assumption that the current-dependent loss is resistive, i.e.,

$$P_d = Ri^2 \tag{51}$$

where R includes the stator coil resistance of the generator and an approximate transmission resistance for the drive. From $v = \mathbf{C}\mathbf{x}$ and Eq. (51), Eq. (50) would be

$$\begin{aligned} P_g &= -\{iv + Ri^2\} \\ &= -\begin{bmatrix} \mathbf{x} \\ i \end{bmatrix}^T \begin{bmatrix} \mathbf{0} & \frac{1}{2}\mathbf{C}^T \\ \frac{1}{2}\mathbf{C} & R \end{bmatrix} \begin{bmatrix} \mathbf{x} \\ i \end{bmatrix} \end{aligned} \tag{52}$$

To maximize the averaged value of Eq. (52) denoted by $\bar{P}_g$, the admittance Y and the tuning spring stiffness k_t are treated as control gains subjected to a white noise

11

input as in [35]. Substituting Eqs. (47) and (48) into Eq. (45) yields the closed loop system

$$\dot{\mathbf{x}} = (\mathbf{A} - Y\mathbf{BC} + k_t\mathbf{FT})\mathbf{x} + \mathbf{G}w \tag{53}$$

In this study, the static admittance control strategy introduced in [33] is utilized for the current i. Thus both Y and k_t are treated as constant values. Therefore in stationary stochastic response, the average power generation $\bar{P}_g$ is given by [36]

$$\bar{P}_g = -\mathbf{G}^T\mathbf{SG} \tag{54}$$

where the covariance matrix $\mathbf{S} = \varepsilon[\mathbf{x}\mathbf{x}^T]$ is computed as the solution to the Lyapunov equation

$$(\mathbf{A} - Y\mathbf{BC} + k_t\mathbf{FT})^T\mathbf{S} + \mathbf{S}(\mathbf{A} - Y\mathbf{BC} + k_t\mathbf{FT}) + \mathbf{C}^T(-Y + Y^2R)\mathbf{C} = 0 \tag{55}$$

For an ideal system, the admittance value to control the input current to the generated is restricted by

$$Y \in [0, 1/R] \tag{56}$$

to assure the definiteness of $\mathbf{S}$. Thus, the objective becomes the optimization of Y and k_t to maximize $\bar{P}_g$.

4. Numerical simulations

To validate the power generation performance of the point absorber with TIM proposed in Fig. 2, numerical studies are carried out and compared with the conventional SDOF system illustrated in Fig. 1. A reasonable size cylindrical buoy with diameter 5 m, draft 1 m, in water depth 30 m is considered. The hydrodynamic coefficients are calculated with the software WAMIT [37] which uses boundary element method based on linear potential theory. The resulting added mass $m_a(\omega)$, radiation damping $c_r(\omega)$, and the magnitude and phase of the transfer function $F_a(\omega)$ defined by Eq. (4) are shown in Fig. 4. The parameters for the generator and buoy used in this study are summarized in Table 1.

Fig. 5 shows the frequency response data G_a and G_f given by Eq. (25) and (26), respectively, and the finite dimensional approximations expressed by Eq. (27). For accuracy, G_a is approximated with 6 zeros and 7 poles, and G_f is approximated with 3 zeros and 4 poles. The wave amplitude a is taken to be the wave amplitude $d = 10$ m ahead of the buoy in the propagation direction. It can be seen that the approximated model matches the frequency response data very well over the dominant wave frequencies.

12

Table 1: Parameter values used for numerical simulation studies

	Parameters	Values
Buoy mass	M	4000 kg
Buoy diameter	D	5 m
Buoy height	H	2 m
Buoy draft	L	1 m
Mechanical damping	c_s	50 N s/m
Supporting spring stiffness	k_s	1.0×10^3 N/m
Electromechanical coupling	K_e	500 V s/m
Resistance	R	25 Ω
Sea water density	ρ	1027 kg/m^3

Previous studies which consider irregular waves typically select some number of sea states as representatives of a deployment site. While, in this study, a more comprehensive analysis is carried out, focussing on the variation of peak wave periods since the system's amplitude response strongly depends on this characteristic parameter. Therefore, stochastic sea state models are determined for each sea state with peak wave period ranging from 2 s to 12 s and $H_s = 1$ m, $\gamma = 1$ for the JONSWAP spectrum defined by Eq. (19).

4.1. TIM system

4.1.1. Design

For the proposed TIM system, the design parameters Y and k_t must be decided for the rotational inertial mass employed. In this study, a rotational inertial mass of $m_s = 8264$ kg is examined which corresponds to 30% of the effective oscillating mass $M + m_\infty$ where m_∞ denotes the infinite frequency added mass having the value of 23,547 kg. This large inertial mass can be realized by a relatively small physical mass due to the rotational amplifying effect [24].

It is well understood that the damping coefficient C_{PTO} strongly affects the magnitude of the generated power. This can be adjusted through the admittance Y of the electronics, thus the damping can be optimized for each sea state. On the other hand, adjusting the stiffness of the tuning spring after deployment is regarded as unpractical. Therefore, the value for k_t is decided so that the power generation is maximized for the predominant sea state assumed as JONSWAP spectrum with $T_p = 6$ s. The optimized value of k_t is obtained through the contour plot shown in
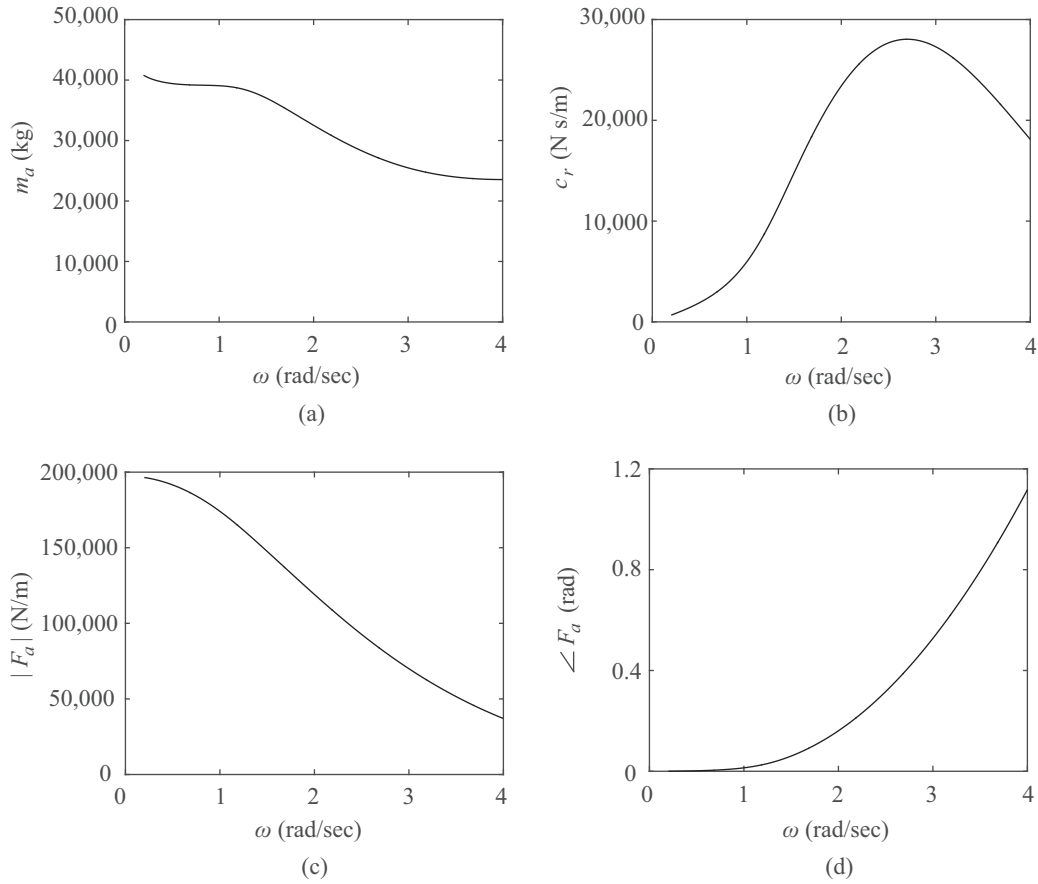
13

Figure 4: Hydrodynamic parameters for the heave mode of a circular cylinder with radius 2.5 m, draft 1 m, in water depth 30 m: (a) Added mass, (b) Radiation damping, (c) Magnitude of $F_a(\omega)$, (d) Phase of $F_a(\omega)$.

Fig. 6, which demonstrates how the admittance and tuning spring stiffness relate to the power generation. The upper limit of k_t is set to 1.0×10^5 N/m which is large enough to consider the spring to be rigid, while the admittance is constrained by Eq. (56). The contour plot shows a clear peak at $k_t = 1.72 \times 10^4$ N/m and $Y = 0.0044 \; \Omega^{-1}$ giving maximum power of $\bar{P}_g = 1795$ W. Hence, the optimum tuning spring stiffness is set to $k_t^* = 1.72 \times 10^4$ N/m and held fixed for the varying sea states.

In the following simulation, the effect of adjusting the rotational inertial mass after deployment is also explored. Therefore, two more values, $m_s = 5509$ kg
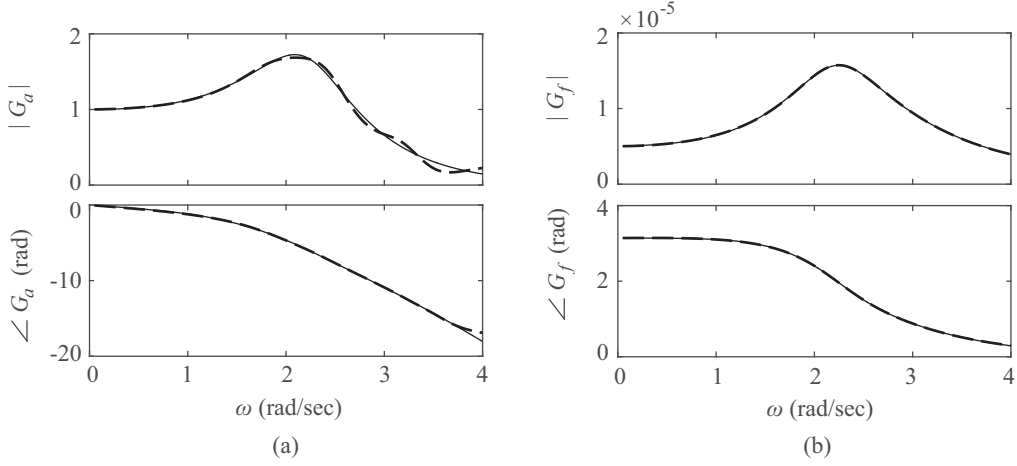
Figure 5: Frequency domain data (solid) and finite-dimensional approximation (dashed) with spatial delay of $d = 10$ m: (a) $G_a(\omega)$, (b) $G_f(\omega)$.

and 11019 kg corresponding to 20% and 40% of the effective oscillating mass are considered. Note, the value of m_s can be adjusted by either changing the attached mass or the radius in which it rotates.

4.1.2. Result

The magnitudes of the transfer functions H_b and H_r defined by Eqs. (43) and (44) with the obtained optimum value $k_t^* = 1.72 \times 10^4$ N/m are compared in Fig. 7. The damping coefficient is set to the optimum value for $T_p = 6$ s in each plot. For the SDOF system, an inertial mass of $m_s = 50$ kg caused by the generator and pulley is assumed. Fig. 7 shows that the amplitude response of the rotational inertial mass is significantly higher than the buoy response, indicating that the tuning spring amplifies the oscillation of the rotational inertial mass compared to the buoy. This leads to increased amplitude and velocity of the generator movement due to its rigid connection with the rotational inertial mass. Moreover, the frequency for optimum amplitude response of the TIM system decreases with increasing m_s. This points out that even when the buoy's natural frequency is apart from the dominant wave frequency, enhanced amplitude response can be gained, and shifting of the frequency is possible through the value of the rotational inertial mass.

Fig. 8 shows the power generation for various sea states, with the optimum damping coefficient given below. It can be clearly seen that all three TIM systems
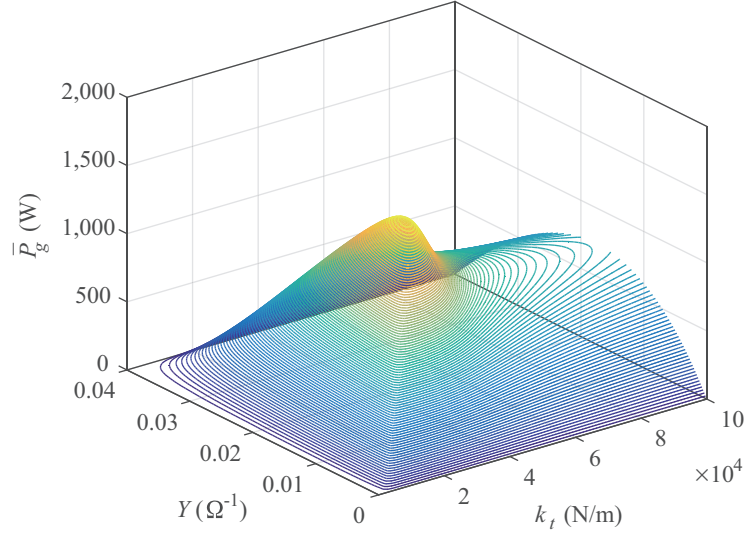
15

Figure 6: Contour plot of power generation showing the effects of the tuning spring stiffness k_t and admittance Y. The plots are for $m_s = 8264$ kg with sea state $T_p = 6$ s, $H_s = 1$ m, $\gamma = 1$.

perform better than the SDOF system, due to the increased amplitude and velocity of the rotational inertial mass and generator. This results in lowering the optimum damping coefficient, opening up the possibility to have small generator units. Furthermore, when the value of m_s is changed, the peak of the power curve is shifted, which indicates that adjusting the rotational inertial mass allows the TIM system to correspond to the variability of T_p.

4.2. Phase controlled TIM system

4.2.1. Design

Considering the significant effect of the TIM system observed from the amplitude response, a superior effect can be expected for when the oscillation of the buoy itself is large, i.e., when the buoy resonates with the wave. In the following example, the effectiveness of the TIM system is validated for when the buoy's natural frequency coincides with the dominant wave period. To shift the heave oscillating period, we assume phase control is applied by adding a fully submerged body [22, 38]. The supplementary inertia due to the submerged body mass and added mass allows the buoy to resonate with the dominating sea state. By placing the submerged body at sufficient depth, the radiation damping and excitation force remains the same with the case of the single cylinder, which is explored before.
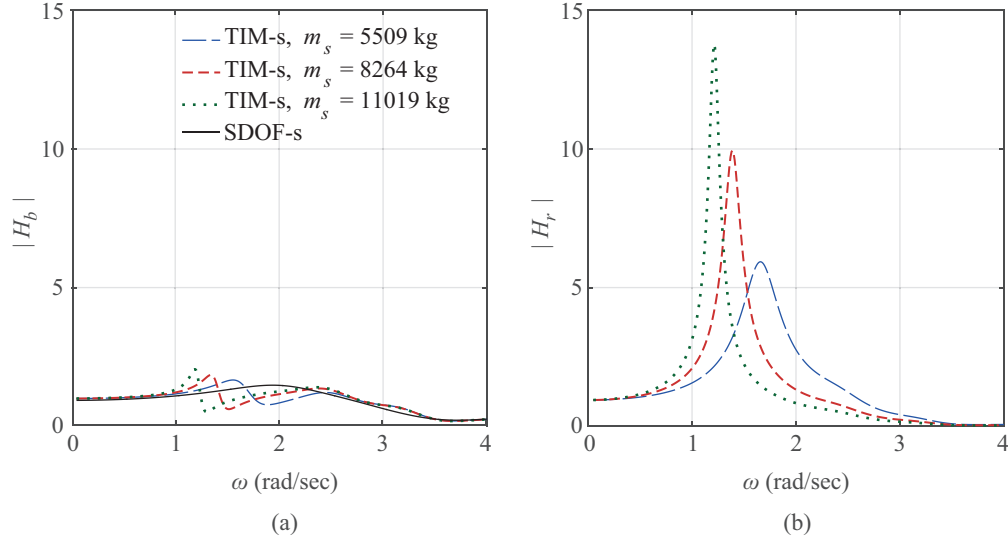
16

Figure 7: The amplitude of the transfer functions when the tuning spring stiffness is $k_t^* = 1.72 \times 10^4$ N/m and the damping coefficient C_{PTO} is set to the optimum value for $T_p = 6$ s, (a) $H_b(\omega)$, (b) $H_r(\omega)$.

The performance of the TIM system is compared with the SDOF system, having the buoy for both systems to be in resonance with the wave motion. Thus, the supplementary inertia due to the submerged body mass and added mass is set to 200×10^3 kg to make the buoy's oscillation tuned to the sea state of $T_p = 6$ s. Fig. 9 shows the finite dimensional approximation of the frequency response data G_a and G_f with the same orders, displaying a distinct peak at 0.9 rad/s due to the resonance of the buoy. For the rotational inertial mass, the same three values (i.e., $m_s = 5509$ kg, $m_s = 8264$ kg, and $m_s = 11019$ kg) are considered. The optimization of the design parameters are carried out in a similar process, following the amplitude response and power generation.

The stiffness of the tuning spring k_t is optimized through the contour plot given in Fig. 10. A sharper peak can be observed at $k_t = 6.06 \times 10^3$ N/m and $Y = 0.0036$ Ω^{-1} giving maximum power of $\bar{P}_g = 17.1$ kW. Hence, the optimum tuning spring stiffness is set to $k_t^* = 6.06 \times 10^3$ N/m.

4.2.2. Result

The amplitude response of the buoy and the rotational inertial mass are shown in Fig. 11. The solid line in Fig. 11(a) shows that the amplitude response of
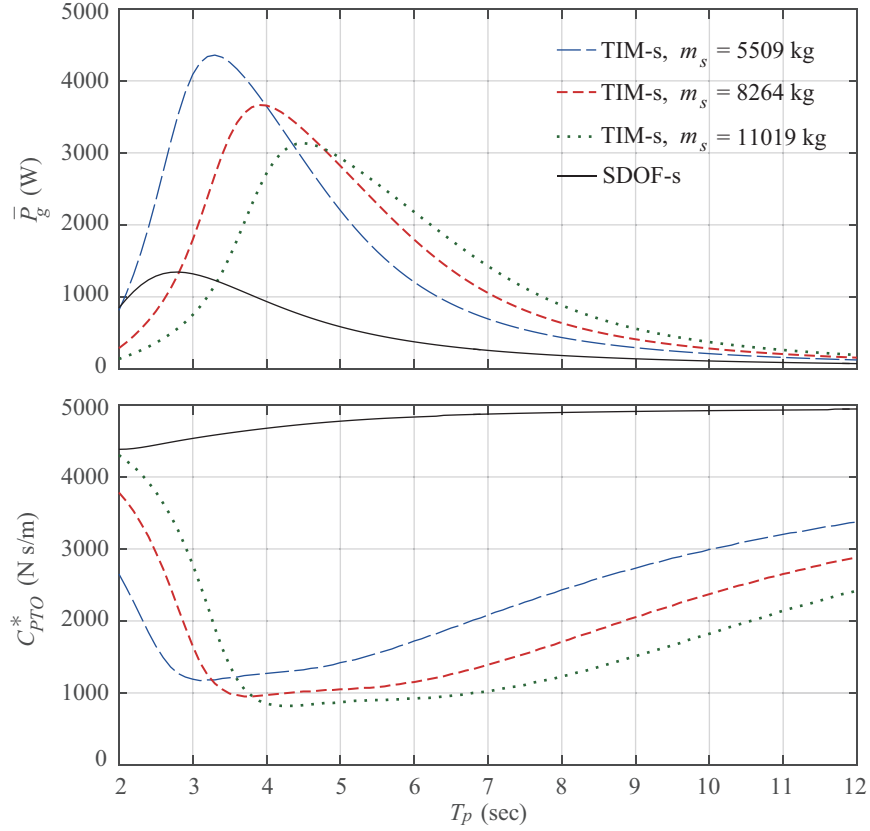
Figure 8: Power generation with optimum damping for each sea state. The tuning spring for the TIM system is set to $k_t^* = 1.72 \times 10^4$ N/m.

the SDOF buoy is greatly enhanced due to phase control, while the bandwidth has become narrow. This has always been an issue associated with the design of point absorbers since a compromise must be made between maximum amplitude response and wide resonance bandwidth over the dominant wave frequencies. On the other hand, the significant effect of the TIM system is that enhanced amplitude response and widened bandwidth is gained at the same time as shown in Fig. 11(b). Especially for the TIM system with $m_s = 8264$ kg in which the tuning spring was optimized, the benefit of 2DOF is gained, considerably widening the bandwidth. We must emphasize that for the proposed TIM system, increased amplitude response of the rotational inertial mass is desired since the generator is coupled to its displacement. While the buoy's amplitude response is reduced for
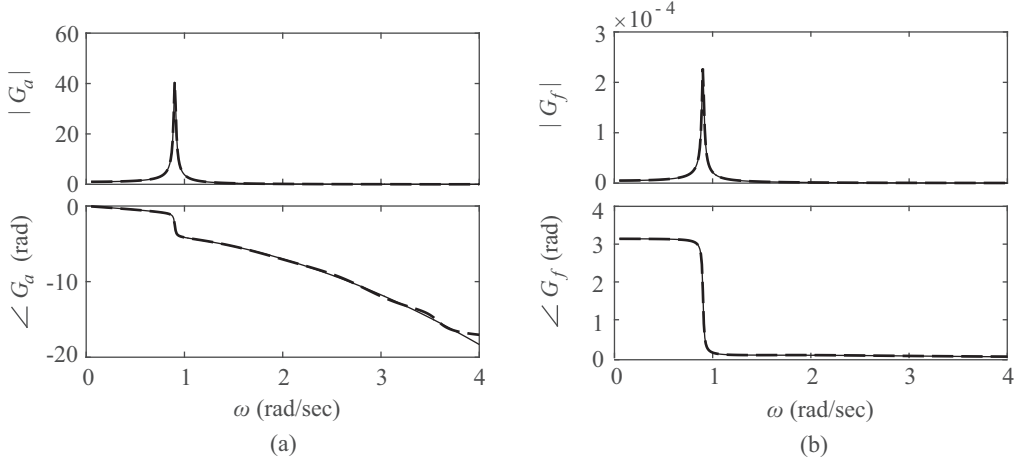
18

Figure 9: Frequency domain data (solid) and finite-dimensional approximation (dashed) with spatial delay of $d = 10$ m: (a) $G_a(\omega)$, (b) $G_f(\omega)$

the TIM system, the amplitude response of the rotational inertial mass is significantly increased. This indicates that a large amount of energy from the wave to the buoy is successfully transferred to the rotational inertial mass for the TIM system.

The power generation of the two systems with phase control is compared in Fig. 12. A similar feature with the amplitude response can be observed, with the TIM system having increased power generation and widened bandwidth. Particularly for the sea state in which resonance is gained, the power generation for the TIM system is increased to more than two times the power of the SDOF system. Contrary to the non-resonant case, the effect of adjusting the rotational inertial mass can not be observed, which indicates that designing k_t for a particular m_s value is sufficient to gain the benefit of the TIM system. As with previous results, a decrease in optimum damping coefficient can be observed for the TIM system, while the optimum damping is less sensitive to the variation of the sea states.

5. Conclusions

A theoretical model for a point absorber with tuned inertial mass has been proposed. Numerical simulations in stochastic sea states using the JONSWAP spectrum were carried out to compare the power generation of the proposed device with the conventional SDOF point absorber. For the TIM system with the buoy's natural frequency apart from the dominant wave frequency, increased power gen-
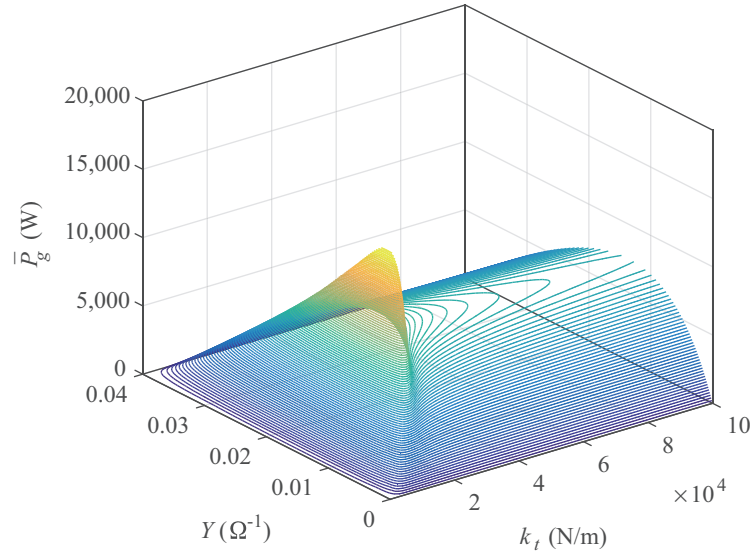
19

Figure 10: Contour plot of power generation showing the effects of the tuning spring stiffness k_t and admittance Y. The plots are for TIM system applied to a resonant buoy with $m_s = 8264$ kg and supplementary inertia of 200 t. Sea state is $T_p = 6$ s, $H_s = 1$ m, $\gamma = 1$.

eration was gained along with the shifting of the power curve depending on the rotational inertial mass value. On the other hand, for the TIM system with a resonant buoy, a significantly high amplitude response of the rotational inertial mass was gained, while the response of the buoy was reduced. This indicated that substantial wave energy was transferred to the rotational inertial mass, leading to increase the power generation to more than two times the power of the conventional system at the resonance frequency.

For future work, methods to determine the optimum rotational inertial mass should be established, along with its sensitivity to the wave spectrum. In addition, algorithms to control the stiffness and damping of the PTO system with regard to the change of the sea state are desired. Furthermore, experimental investigation [39] to assess the feasibility of the device under real sea condition is required. This includes the consideration of locking the PTO system in survival mode and understanding the buoy response to highly non-linear extreme waves.
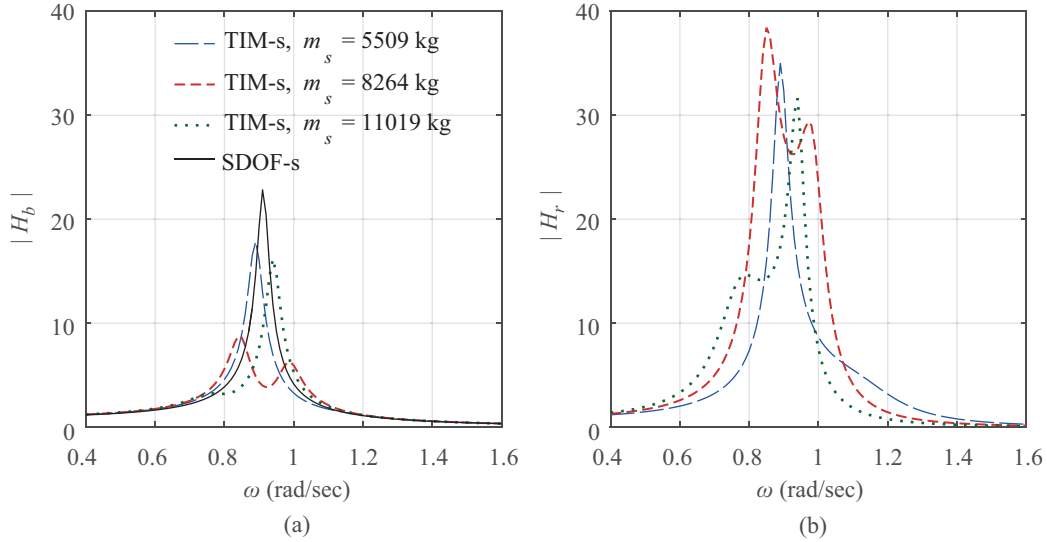
Figure 11: The amplitude of the transfer functions when the tuning spring stiffness is $k_t^* = 6.06 \times 10^3$ N/m and the damping coefficient C_{PTO} is set to the optimum value for $T_p = 6$ s: (a) $H_b(\omega)$, (b) $H_r(\omega)$.

Acknowledgement

References

[1] M. Leijon, H. Bernhoff, M. Berg, O. Ågren, Economical consid-erations of renewable electric energy production—especially develop-ment of wave energy, Renewable Energy 28 (8) (2003) 1201 – 1209. doi:https://doi.org/10.1016/S0960-1481(02)00157-X.

[2] J. Scruggs, P. Jacob, Harvesting ocean wave energy, Science 323 (5918) (2009) 1176–1178. doi:10.1126/science.1168245.

[3] M. McCormick, Ocean Wave Energy Conversion, Dover Civil and Mechan-ical Engineering Series, Dover Publications, 2007.

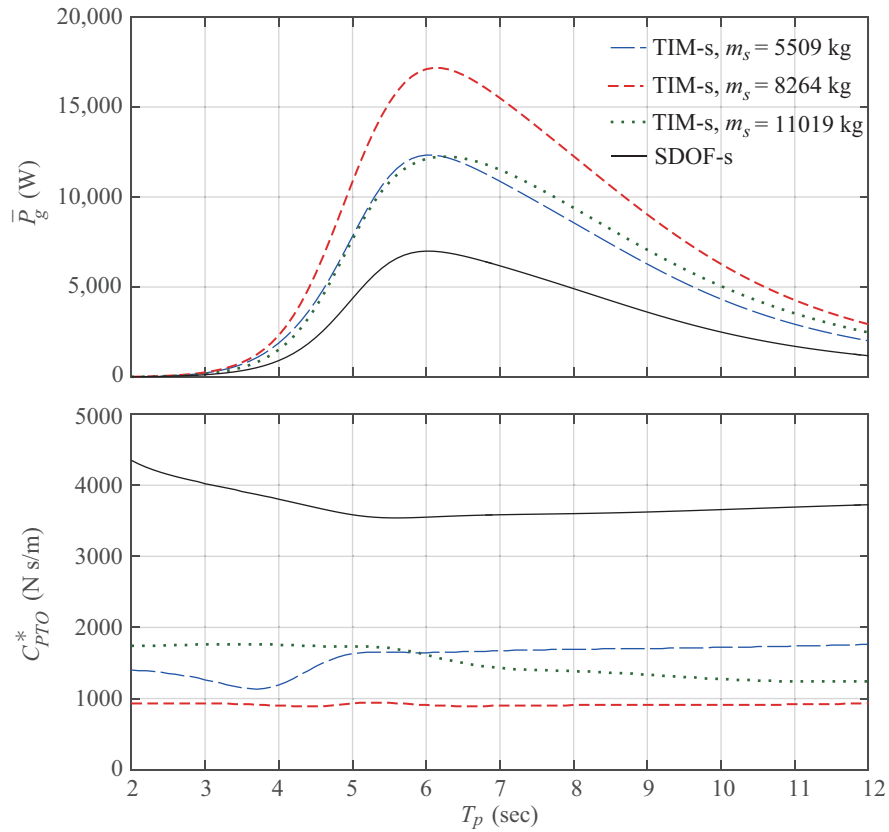Figure 12: Power generation with phase control and optimum damping. For the TIM system, the tuning spring is set to $k_t^* = 6.06 \times 10^3$ N/m.

[4] A. F. de O. Falcão, Wave energy utilization: A review of the technologies, Renewable and Sustainable Energy Reviews 14 (3) (2010) 899 – 918. doi:https://doi.org/10.1016/j.rser.2009.11.003.

[5] J. Falnes, A review of wave-energy extraction, Marine Structures 20 (4) (2007) 185 – 201. doi:https://doi.org/10.1016/j.marstruc.2007.09.001.

[6] A. F. Falcão, J. C. Henriques, Oscillating-water-column wave energy converters and air turbines: A review, Renewable Energy 85 (2016) 1391 – 1424. doi:https://doi.org/10.1016/j.renene.2015.07.086.

[7] L. Margheritini, D. Vicinanza, P. Frigaard, SSG wave energy converter: Design, reliability and hydraulic performance of an innova-

tive overtopping device, Renewable Energy 34 (5) (2009) 1371 – 1380. doi:https://doi.org/10.1016/j.renene.2008.09.009.

[8] N. Guillou, G. Chapalain, Annual and seasonal variabilities in the performances of wave energy converters, Energy 165 (2018) 812 – 823. doi:https://doi.org/10.1016/j.energy.2018.10.001.

[9] J. Morim, N. Cartwright, M. Hemer, A. Etemad-Shahidi, D. Strauss, Inter- and intra-annual variability of potential power production from wave energy converters, Energy 169 (2019) 1224 – 1241. doi:https://doi.org/10.1016/j.energy.2018.12.080.

[10] E. Rusu, F. Onea, A review of the technologies for wave energy extraction, Clean Energy 2 (1) (2018) 10–19. doi:10.1093/ce/zky003.

[11] Y. Li, Y.-H. Yu, A synthesis of numerical methods for modeling wave energy converter-point absorbers, Renewable and Sustainable Energy Reviews 16 (6) (2012) 4352 – 4364. doi:https://doi.org/10.1016/j.rser.2011.11.008.

[12] K. Budar, J. Falnes, A resonant point absorber of ocean-wave power, Nature 256 (5517) (1975) 478.

[13] M. Eriksson, J. Isberg, M. Leijon, Hydrodynamic modelling of a direct drive wave energy converter, International Journal of Engineering Science 43 (17) (2005) 1377 – 1387. doi:https://doi.org/10.1016/j.ijengsci.2005.05.014.

[14] K. Budal, J. Falnes, Wave power conversion by point absorbers: A norwegian project, International Journal of Ambient Energy 3 (2) (1982) 59–67. doi:10.1080/01430750.1982.9675829.

[15] W. Sheng, R. Alcorn, A. Lewis, On improving wave energy conversion, part i: Optimal and control technologies, Renewable Energy 75 (2015) 922 – 934. doi:https://doi.org/10.1016/j.renene.2014.09.048.

[16] A. Babarit, G. Duclos, A. Clément, Comparison of latching control strategies for a heaving wave energy device in random sea, Applied Ocean Research 26 (5) (2004) 227 – 238. doi:https://doi.org/10.1016/j.apor.2005.05.003.

[17] I. Temiz, J. Leijon, B. Ekergård, C. Boström, Economic aspects of latching control for a wave energy converter with a direct drive linear generator power take-off, Renewable Energy 128 (2018) 57 – 67. doi:https://doi.org/10.1016/j.renene.2018.05.041.

[18] J. H. Todalshaug, G. S. Ásgeirsson, E. Hjálmarsson, J. Maillet, P. Möller, P. Pires, M. Guérinel, M. Lopes, Tank testing of an inherently phase-controlled wave energy converter, International Journal of Marine Energy 15 (2016) 68 – 84, selected Papers from the European Wave and Tidal Energy Conference 2015, Nante, France. doi:https://doi.org/10.1016/j.ijome.2016.04.007.

[19] E. Anderlini, D. Forehand, E. Bannon, M. Abusara, Reactive control of a wave energy converter using artificial neural networks, International Journal of Marine Energy 19 (2017) 207 – 220. doi:https://doi.org/10.1016/j.ijome.2017.08.001.

[20] J. Xie, L. Zuo, Dynamics and control of ocean wave energy converters, International Journal of Dynamics and Control 1 (3) (2013) 262–276. doi:10.1007/s40435-013-0025-x.

[21] M. Shadman, S. F. Estefen, C. A. Rodriguez, I. C. Nogueira, A geometrical optimization method applied to a heaving point absorber wave energy converter, Renewable Energy 115 (2018) 533 – 546. doi:https://doi.org/10.1016/j.renene.2017.08.055.

[22] J. Engström, M. Eriksson, J. Isberg, M. Leijon, Wave energy converter with enhanced amplitude response at frequencies coinciding with swedish west coast sea states by use of a supplementary submerged body, Journal of Applied Physics 106 (6) (2009) 064512. doi:10.1063/1.3233656.

[23] J. Den Hartog, Mechanical Vibrations, Dover Civil and Mechanical Engineering, Dover Publications, 2013.

[24] K. Ikago, K. Saito, N. Inoue, Seismic control of single-degree-of-freedom structure using tuned viscous mass damper, Earthquake Engineering & Structural Dynamics 41 (3) 453–474. doi:10.1002/eqe.1138.

[25] T. Asai, Y. Araki, K. Ikago, Structural control with tuned inertial mass electromagnetic transducers, Structural Control and Health Monitoring 25 (2) e2059, e2059 stc.2059. doi:10.1002/stc.2059.

[26] T. Asai, Y. Watanabe, Outrigger tuned inertial mass electromagnetic transducers for high-rise buildings subject to long period earthquakes, Engineering Structures 153 (2017) 404 – 410. doi:https://doi.org/10.1016/j.engstruct.2017.10.040.

[27] J. Falnes, Ocean Waves and Oscillating Systems: Linear Interactions Including Wave-Energy Extraction, Cambridge University Press, 2002. doi:10.1017/CBO9780511754630.

[28] A. M. Miquel, A. Antonini, R. Archetti, S. Bozzi, A. Lamberti, Non-linear modelling of a heaving point absorber: The surge effect, International Journal of Marine Energy 19 (2017) 95 – 109. doi:https://doi.org/10.1016/j.ijome.2017.07.002.

[29] I. L. Cassidy, J. T. Scruggs, Nonlinear stochastic controllers for power-flow-constrained vibratory energy harvesters, Journal of Sound and Vibration 332 (13) (2013) 3134 – 3147. doi:https://doi.org/10.1016/j.jsv.2013.01.023.

[30] R. R. Krishnan, Electric motor drives : modeling, analysis, and control, Upper Saddle River, N.J. : Prentice Hall, 2001, includes bibliographical references and index.

[31] O. Faltinsen, Sea Loads on Ships and Offshore Structures, Cambridge Ocean Technology Series, Cambridge University Press, 1993.

[32] P.-T. Spanos, Filter approaches to wave kinematics approximation, Applied Ocean Research 8 (1) (1986) 2 – 7. doi:https://doi.org/10.1016/S0141-1187(86)80025-6.

[33] J. Scruggs, S. Lattanzio, A. Taflanidis, I. Cassidy, Optimal causal control of a wave energy converter in a random sea, Applied Ocean Research 42 (2013) 1 – 15. doi:https://doi.org/10.1016/j.apor.2013.03.004.

[34] J. Falnes, On non-causal impulse response functions related to propagating water waves, Applied Ocean Research 17 (6) (1995) 379 – 389. doi:https://doi.org/10.1016/S0141-1187(96)00007-7.

[35] T. Asai, Y. Araki, K. Ikago, Energy harvesting potential of tuned inertial mass electromagnetic transducers, Mechanical Systems and Signal Processing 84 (2017) 659 – 672. doi:https://doi.org/10.1016/j.ymssp.2016.07.048.

[36] P. Dorato, V. Cerone, C. Abdallah, Linear-Quadratic Control: An Introduction, Simon & Schuster, Inc., New York, NY, USA, 1994.

[37] WAMIT, Inc., WAMIT, http://www.wamit.com/index.htm, MA, USA (2020).

[38] J. Engström, V. Kurupath, J. Isberg, M. Leijon, A resonant two body system for a point absorbing wave energy converter with direct-driven linear generator, Journal of Applied Physics 110 (12) (2011) 124904. doi:10.1063/1.3664855.

[39] K. Sugiura, R. Sawada, Y. Nemoto, R. Haraguchi, T. Asai, Wave flume testing of an oscillating-body wave energy converter with a tuned inerter, Applied Ocean Research 98 (2020) 102127. doi:https://doi.org/10.1016/j.apor.2020.102127.